nature medicine

Commensal microbiota affects ischemic stroke outcome by regulating intestinal γδ T cells

Corinne Benakis[1,5], David Brea[1,5], Silvia Caballero[2,3], Giuseppe Faraco[1], Jamie Moore[1], Michelle Murphy[1], Giulia Sita[1], Gianfranco Racchumi[1], Lilan Ling[4], Eric G Pamer[2–4], Costantino Iadecola[1] & Josef Anrather[1]

Commensal gut bacteria impact the host immune system and can influence disease processes in several organs, including the brain. However, it remains unclear whether the microbiota has an impact on the outcome of acute brain injury. Here we show that antibiotic-induced alterations in the intestinal flora reduce ischemic brain injury in mice, an effect transmissible by fecal transplants. Intestinal dysbiosis alters immune homeostasis in the small intestine, leading to an increase in regulatory T cells and a reduction in interleukin (IL)-17–positive γδ T cells through altered dendritic cell activity. Dysbiosis suppresses trafficking of effector T cells from the gut to the leptomeninges after stroke. Additionally, IL-10 and IL-17 are required for the neuroprotection afforded by intestinal dysbiosis. The findings reveal a previously unrecognized gut-brain axis and an impact of the intestinal flora and meningeal IL-17$^+$ γδ T cells on ischemic injury.

Ischemic stroke is a highly prevalent disease with limited therapeutic options[1]. Inflammation is a key component in the pathophysiology of cerebral ischemia[2], and numerous experimental approaches have explored the therapeutic potential of immunomodulation[3]. However, our understanding of the interaction between resident brain cells and the peripheral immune cells that infiltrate the post-ischemic brain, and their role in tissue damage and repair, is still incomplete[3]. The peripheral immune system, which involves both innate and adaptive immune cells, has an essential role in the pathophysiology of stroke and contributes to secondary neurodegeneration by releasing neurotoxic factors, including reactive oxygen and nitrogen species, as well as exopeptidases[2].

The continuous interaction between the immune system and the commensal microbes that populate epithelial surfaces is essential for immune cell development, maintenance and function[4]. Intestinal commensal microbes, the most abundant symbiotic compartment in the body, have emerged as a potent regulator of lymphocyte populations, including regulatory T (T_{reg}) and γδ T cells, both of which are involved in cerebral ischemic injury[2]. γδ T cells, a major lymphocyte population with innate immune features, are located at epithelial surfaces, including the intestine[5]. They can aggravate ischemic brain injury by secreting IL-17 and generating chemotactic signals for peripheral myeloid cells, such as neutrophils and monocytes[6,7]. Although these studies suggested a causal involvement of IL-17$^+$ γδ T cells in ischemic brain injury, their origin and site of action have not been clearly elucidated. While effector T cells may contribute to focal ischemic injury, T_{reg} cells can contribute to neuroprotection by downregulating post-ischemic inflammation[8]. T_{reg} cells appear in the ischemic tissue after the acute phase and confer neuroprotection by secreting the anti-inflammatory cytokine IL-10, an effect thought to be antigen independent[9,10]. Despite exerting a protective effect, adoptively transferred T_{reg} cells do not enter the brain parenchyma in the acute phase of stroke[11], suggesting that T_{reg} cells exert their beneficial effect by modulating the peripheral immune system rather than by acting on brain tissue directly[11]. Intestinal T_{reg} cells are indispensable for maintaining an anti-inflammatory environment in the gut by suppressing the differentiation of T helper (T_H) 17 cells[12,13] and the proliferation of γδ T cells[14]. In this study we investigated the effects of altered intestinal flora on the immune system and the outcome after cerebral ischemia.

RESULTS

Ischemic brain injury is reduced in mice with an altered intestinal flora

To modify the composition of the gut microbiota, we treated male C57BL/6 mice for 2 weeks with the antibiotics amoxicillin and clavulanic acid (AC) to select against AC-sensitive (AC^{Sens}) flora (**Fig. 1a** and **Supplementary Fig. 1a**). To control for off-target antibiotic effects, we established a mouse model that could be kept under antibiotic treatment without altering the intestinal flora. This was accomplished by co-housing experimental mice that were undergoing AC treatment with seeder mice, which carry an AC-resistant (AC^{Res}) gut microflora that is qualitatively similar to the one found in naive animals (**Supplementary Fig. 1b**). Because of the coprophagic behavior of mice, the AC^{Res} flora is successfully transmitted to the naive mice. Thus, AC-treated mice co-housed with these seeder animals

[1]Feil Family Brain and Mind Research Institute, Weill Cornell Medical College, New York, New York, USA. [2]Immunology Program and Infectious Disease Service, Memorial Sloan Kettering Cancer Center, New York, New York, USA. [3]Immunology and Microbial Pathogenesis Program, Weill Cornell Graduate School of Medical Sciences, New York, New York, USA. [4]Lucille Castori Center for Microbes, Inflammation and Cancer, Memorial Sloan Kettering Cancer Center, New York, New York, USA. [5]These authors contributed equally to this work. Correspondence should be addressed to J.A. (joa2006@med.cornell.edu).

Received 26 November 2015; accepted 17 February 2016; published online 28 March 2016; doi:10.1038/nm.4068

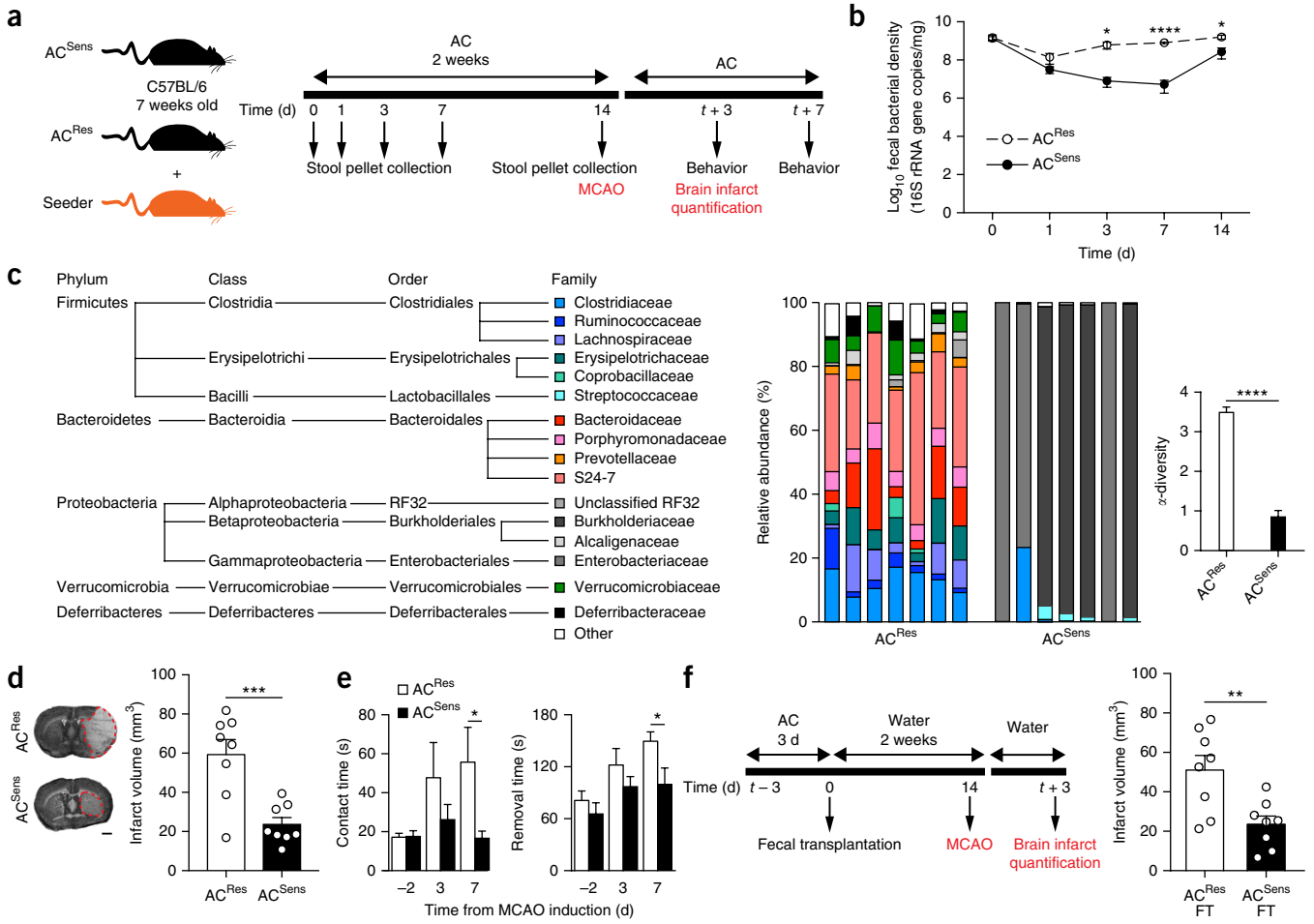

Figure 1 Alteration of intestinal microbiota protects from MCAO-induced brain injury. (**a**) Experimental design of AC treatment in 7-week-old C57BL/6 mice. Both AC^{Sens} mice and AC^{Res} mice co-housed with AC^{Res} seeder mice received antibiotics via drinking water for 2 weeks. Stool collection time points are indicated. MCAO is induced after 2 weeks of AC treatment, and brain infarct volume is quantified 3 d later. Other groups of mice are assessed for sensorimotor function. (**b**) Fecal r16S DNA copy numbers in AC^{Res} and AC^{Sens} mice ($n = 5$ per group). (**c**) Left and middle, family-level phylogenetic classification (left) of fecal 16S rDNA gene frequencies from AC^{Res} and AC^{Sens} mice that were treated with antibiotics for 2 weeks (middle). Each bar represents an individual animal. Right, graph depicts Shannon α-diversity index of grouped data ($n = 7$ mice per group). Only families with a frequency >1% were included. (**d**) Representative images of Nissl-stained coronal brain sections (left) and quantification of infarct volumes (right) in AC^{Res} and AC^{Sens} mice 3 d after MCAO induction ($n = 8$ mice per group). Scale bar, 1 mm. (**e**) Sensorimotor function in AC^{Res} and AC^{Sens} mice. Graphs show contact time (left) and time to removal of the tape (right) from the contralateral forepaw 2 d before, and 3 d and 7 d after MCAO induction ($n = 11$ mice per group). (**f**) Left, fecal transplant (FT) experimental design. Mice were pulse-treated with AC for 3 d and gavaged with cecal contents from either AC^{Res} or AC^{Sens} donors. After 2 weeks on water, MCAO was induced in the FT recipient mice, and they were killed 3 d later to quantify infarct volume. Right, infarct volumes in FT recipient mice ($n = 8$ mice per group). Throughout, error bars represent mean ± s.e.m. $^*P < 0.05$, $^{**}P < 0.01$, $^{***}P < 0.001$, $^{****}P < 0.0001$; by Student's t-test.

acquire an AC^{Res} microbiota (hereafter referred to as AC^{Res} mice) (**Fig. 1a**, **Supplementary Fig. 1** and **Supplementary Data**). AC treatment reduced fecal bacterial copies for the first 3 d of treatment in mice with AC^{Sens} flora (which we refer to as AC^{Sens} mice), but bacterial numbers recovered after 2 weeks of AC treatment, reflecting gut colonization of these mice with AC-insensitive bacterial species (**Fig. 1b**). No major changes in biomass were observed in AC^{Res} mice, indicating a seamless transition from AC-sensitive to AC-resistant flora (**Fig. 1b**). Phylogenetic analysis 2 weeks after the start of AC treatment revealed an alteration in the composition of the gut microbiota in AC^{Sens} mice, with an overall reduction in the diversity of intestinal microbial populations (α-diversity), an expansion in members of Proteobacteria and a contraction in Firmicutes and Bacteroidetes (**Fig. 1c**).

We induced transient middle cerebral artery occlusions (MCAO) in our mice and found a 60% ± 6% reduction in infarct volume in AC-treated mice with AC^{Sens} flora, as compared to AC-treated mice with AC^{Res} flora (**Fig. 1d**). Sensorimotor function was better preserved in AC^{Sens} than in AC^{Res} mice 3 d and 7 d after ischemia (**Fig. 1e**). This protective effect was not limited to this particular model of dysbiosis. Protection was also observed in mice treated with vancomycin, an antibiotic that is poorly absorbed by the gastrointestinal tract, even when treatment was discontinued 3 d before MCAO induction, to eliminate possible systemic effects of antibiotic treatment (**Supplementary Fig. 2a**,**b**). The vancomycin-induced changes in the composition of the intestinal flora were similar to those of AC^{Sens} animals (**Supplementary Fig. 2c**), supporting the hypothesis that alterations in the intestinal flora result in neuroprotection. Body weight, rectal temperature and intra-occlusion cerebral blood flow (CBF) did not differ among groups. Reperfusion CBF varied widely between groups, but, as reported in other models[15,16], it had

no relationship with the size of the infarct (**Supplementary Fig. 3** and **Supplementary Table 1**). To assess whether the protective effect of intestinal dysbiosis was due to alterations in the blood-brain barrier (BBB), which is altered in germ-free mice[17], we investigated BBB permeability and found no difference between AC^{Res} and AC^{Sens} mice either at baseline or 6 h after stroke, suggesting that alterations in BBB integrity did not account for the protection observed in AC^{Sens} mice (**Supplementary Fig. 4**).

To assess whether these neuroprotective effects were directly mediated by the gut flora, we performed single fecal transplants by transferring the flora from AC^{Res} or AC^{Sens} mice to mice that were pulse-treated with AC for 3 d (**Fig. 1f**). We induced MCAO in the mice 14 d after the transplant and found a 54% ± 8% reduction in infarct volume (72 h after MCAO induction) in mice that received fecal transplants from AC^{Sens} mice as compared to that in mice that received transplants from AC^{Res} mice. We observed several commonalities in the microbial communities in antibiotic-treated mice and in mice receiving fecal transplants. Microbial diversity was reduced in mice receiving transplants from AC^{Sens} donors (**Supplementary Fig. 5a**). As in antibiotic-treated mice, Clostridiaceae and Bacteroidetes S24-7, the dominant bacterial families in AC^{Res}-transplanted mice, were reduced in mice receiving AC^{Sens} fecal transplants (**Supplementary Fig. 5a** and **Supplementary Data**). In place of Proteobacteria, we observed an expansion of Lachnospiraceae, Verrucomicrobiaceae and Anaeroplasmataceae. Despite the differences between antibiotic-treated and transplanted mice, the relative frequencies of several bacterial families, including Verrucomicrobiaceae, Prevotellaceae and Clostridiaceae, were identified as good predictors of infarct volume in both treatment paradigms by 'random forest' classification (**Supplementary Fig. 5b** and **Supplementary Data**).

Dysbiosis affects intestinal T_{reg} and IL-17$^+$ γδ T cells

Next we sought to elucidate the mechanisms of the protection exerted by altered gut flora 2 weeks after AC treatment. Ischemic stroke has an inflammatory component that involves peripheral immune cells, including lymphocytes[2]. Among these, T_{reg} cells and IL-17–producing γδ T cells (IL-17$^+$ γδ T) have been implicated in mechanisms of ischemic injury[6,7,9,18]. The intestinal lamina propria (LP) and epithelium contain the largest population of T cells in the body, γδ T cells in particular, and the gut microbiota provide diverse signals for tuning the host immune system toward either an effector or a regulatory phenotype[19,20]. Consequently, we investigated the effects of intestinal dysbiosis on T_{reg} and IL-17–producing T cells in the gut, blood and secondary lymphoid organs. Flow cytometric analysis of intestinal immune cells revealed an increase in CD4$^+$FoxP3$^+$ T_{reg} cells and a reduction in IL-17$^+$ γδ T in the LP of the small intestine of AC^{Sens} mice 2 weeks after commencing treatment, whereas IL-17–producing T helper (T_H17) cells were not affected (**Fig. 2**). Similar changes were observed in intraepithelial T_{reg} cells but not in IL-17$^+$ γδ T cells. Independently of the treatment group, the frequency of IL-17$^+$ γδ T cells was lower in intraepithelial γδ T cells than in γδ T cells of the LP (**Supplementary Fig. 6a**,**b**). Consistent with a selective regional effect of the altered microbiota on immune cell composition in the small intestine, the frequencies of T_{reg} and IL-17$^+$ γδ T cells in the LP of the large intestine (**Fig. 2b**,**d**), peripheral blood, lymph nodes and spleen did not differ among groups (**Supplementary Fig. 7**). As in AC^{Sens} mice, the frequency of IL-17$^+$ γδ T cells in the LP of the small intestine of vancomycin-treated mice was also reduced (**Supplementary Fig. 6c**). To assess the interdependence between the intestinal flora, gut immune cells and infarct volume, we determined these parameters in AC^{Res} and AC^{Sens} mice 1 week after the commencement of antibiotic treatment. Whereas the microbial composition was different 3 d after AC treatment (**Supplementary Fig. 8a** and **Supplementary Data**), the intestinal microbial composition in AC^{Res} and AC^{Sens} mice after 1 week of treatment was similar to that observed after 2 weeks of treatment (**Supplementary Fig. 8b** and **Supplementary Data**), indicating that the microbial community stabilized after 1 week, although bacterial numbers still expanded in AC^{Sens} mice during the second week (**Fig. 1b**). Infarct volume, LP T_{reg} cells and LP IL-17$^+$ γδ T cells were not affected after 1 week of treatment (**Supplementary Fig. 8c**,**d**); changes in the frequency of intestinal T_{reg} and IL-17$^+$ γδ T cells were only apparent after 2 weeks of treatment, when neuroprotection was also observed.

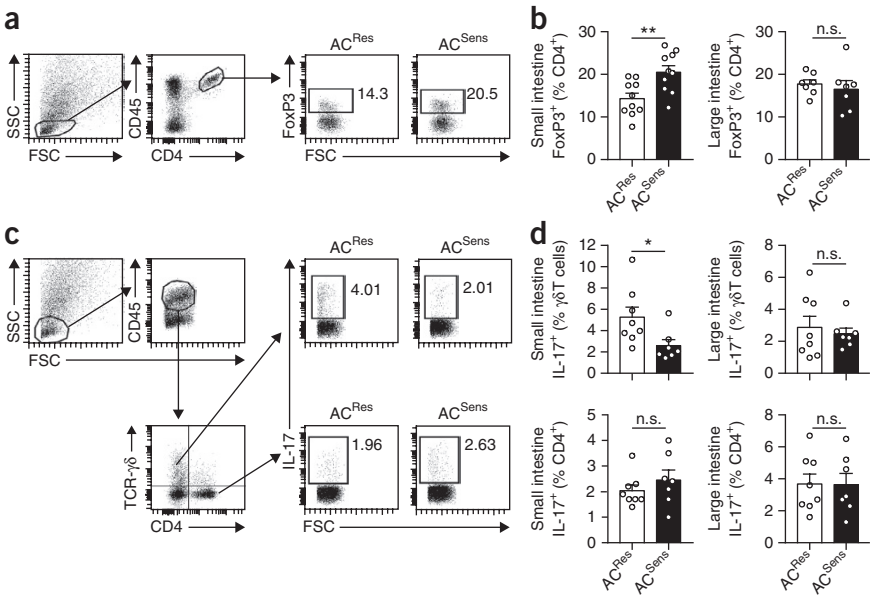

Figure 2 Increased T_{reg} cells and reduced IL-17$^+$ γδ T cells in the small intestine of AC^{Sens} mice. (**a**,**b**) Representative flow cytometry plots of CD4 T cells identified using side scatter (SSC) and forward scatter (FSC) plots (**a**, left) and CD45$^+$ and CD4$^+$ expression (**a**, middle). Representative flow cytometry plots of T_{reg} cells (CD45$^+$CD4$^+$FoxP3$^+$) in the LP of the small intestine (numbers represent events within the gate as a percentage of CD4$^+$ cells) (**a**, right) and quantification of FoxP3$^+$ cells in the LP of the small intestine (n = 10 mice per group) (**b**, left) and large intestine (n = 7 mice per group) (**b**, right) of AC^{Res} and AC^{Sens} mice are shown. (**c**,**d**) Representative flow cytometry analysis of IL-17 production in γδ T cells (CD45$^+$TCR-γδ$^+$CD4$^-$) and CD4$^+$ T cells (CD45$^+$TCR-γδ$^-$CD4$^+$) in the LP of the small intestine (**c**) and quantification of IL-17–producing cells in the LP of the small (**d**, left) and large (**d**, right) intestine of AC^{Res} (n = 8) and AC^{Sens} (n = 7) mice after 2 weeks of antibiotic treatment. The boxes in the dot plots (**c**, right) identify IL-17$^+$ cells, and the numbers represent IL-17$^+$ cells as a percentage of γδ T cells (top right) or CD4$^+$ cells (bottom right) in AC^{Res} and AC^{Sens} mice. Throughout, error bars represent mean ± s.e.m. $^*P < 0.05$; $^{**}P < 0.01$; n.s., not significant; by Student's t-test.

IL-17⁺ γδ T cells accumulate in the meninges after stroke

Next we addressed whether the immune response after stroke was altered in mice with intestinal dysbiosis. Flow cytometric analysis of brain immune cells revealed reduced infiltration of blood-borne cells ($CD45^{high}$) at 2 d and 3 d after reperfusion in AC^{Sens} versus AC^{Res} mice (**Fig. 3a**). Although all leukocyte types were reduced, neutrophils were more prominently diminished at day 2 (**Fig. 3a**). Because post-ischemic neutrophil infiltration contributes to brain injury[21,22], we sought to determine the expression pattern of chemokines that might be involved in neutrophil recruitment in the brain. We found reduced expression of the chemokine genes *Cxcl1* and *Cxcl2* in the brains of AC^{Sens} mice, as compared to that in the brains of AC^{Res} mice 24 h after stroke (**Fig. 3b**). Consistent with reduced neutrophil infiltration in the brain, we observed a trend for increased neutrophil numbers in the meninges of AC^{Sens} mice 48 h after stroke (**Fig. 3c**).

Because IL-17 is a major inducer of the Cxcl1 and Cxcl2 chemokines[6,7], we examined the frequency of IL-17–producing cells in the brain after ischemia. We treated mice that carry the gene encoding green fluorescent protein (GFP) at the endogenous *Il17a* locus (which we refer to as IL-17–GFP mice) according to the AC^{Res} or AC^{Sens}

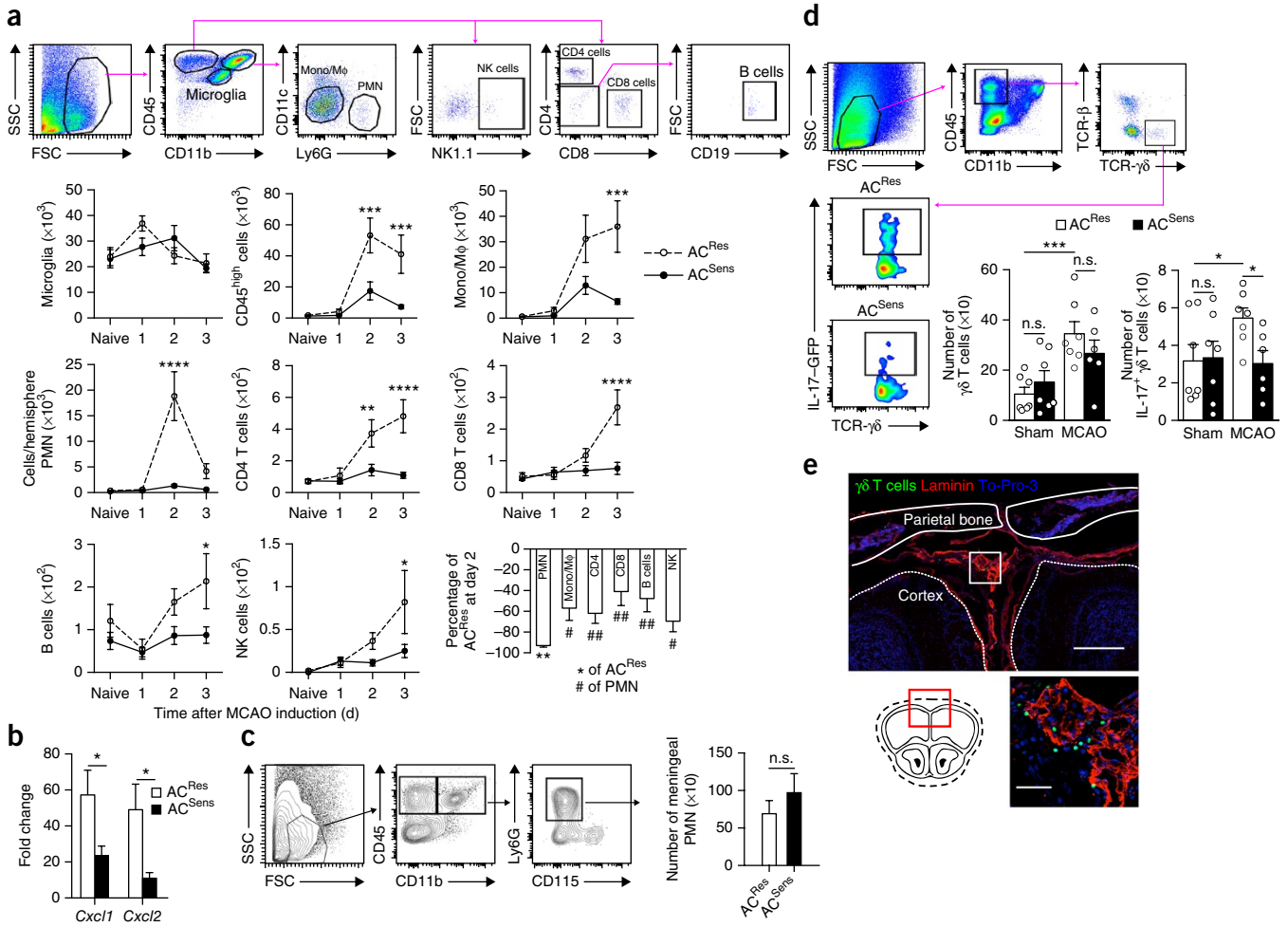

Figure 3 Accumulation of IL-17⁺ γδ T cells at the meninges is associated with increased infarct size. (**a**) Top, flow cytometric gating strategy of brain microglia ($CD45^{int}CD11b^{int}$) and infiltrating leukocytes ($CD45^{high}$)—including monocytes and macrophages (Mono/MΦ; $CD11b^{+}Ly6G^{-}CD11c^{-}$), neutrophils (PMN; $CD11b^{+}Ly6G^{+}CD11c^{-}$), CD4⁺ T cells ($CD11b^{-}CD4^{+}CD8^{-}$), CD8⁺ T cells ($CD11b^{-}CD8^{+}CD4^{-}$), B cells ($CD11b^{-}CD4^{-}CD8^{-}CD19^{+}$) and natural killer cells (NK; $CD11b^{-}NK1.1^{+}$)—in AC^{Res} and AC^{Sens} naive mice and in mice 1 d, 2 d and 3 d after MCAO. Bottom, quantification of the absolute number of cells for each leukocyte subpopulation in the ischemic hemisphere of the brains of naive AC^{Res} and AC^{Sens} mice or of those euthanized on day 1, day 2 or day 3 after MCAO induction ($n = 5$–9 mice per group per time point; **Supplementary Table 3a** shows the exact n values for each group and time point for the different immune cell markers). Bottom right graph shows the percentage of leukocyte reduction in AC^{Sens} mice relative to AC^{Res} mice 2 d after reperfusion (AC^{Sens} PMN, $n = 8$; AC^{Sens} Mono/MΦ, $n = 9$; AC^{Sens} CD4, $n = 9$; AC^{Sens} CD8, $n = 8$; AC^{Sens} B cells, $n = 9$; AC^{Sens} NK, $n = 8$; see **Supplementary Table 3b**). Error bars represent mean ± s.e.m. $^{**}P < 0.01$ versus AC^{Res} mice; $^{\#}P < 0.05$ and $^{\#\#}P < 0.01$ versus neutrophils; by Student's t-test. (**b**) *Cxcl1* and *Cxcl2* mRNA expression in the brains of AC^{Res} and AC^{Sens} mice 1 d after MCAO induction ($n = 10$ mice per group). Values are fold change relative to mRNA expression in the brains of naive mice. (**c**) Representative flow cytometry plots showing gating strategy (left) to quantify (right) meningeal PMN in AC^{Res} and AC^{Sens} mice 1 d after MCAO induction ($n = 9$ mice per group). (**d**) Representative flow cytometry analysis (plots) and quantification of total (left graph) and IL-17⁺ meningeal γδ T cells ($CD45^{high}CD11b^{-}$TCR-β^{-}TCR-γδ^{+}GFP^{+}) (right graph) from AC^{Res} or AC^{Sens} *Il17a-eGFP* mice 16 h after sham surgery ($n = 7$ mice per group) or MCAO induction (AC^{Res}, $n = 7$; AC^{Sens}, $n = 6$). Each data point (n) is derived by pooling two hemispheres. (**e**) Top, representative photomicrograph of meningeal γδ T cells (green; TCR-γδ–GFP⁺), laminin (red) and cell nuclei (blue, To-Pro-3) 16 h after MCAO induction, with magnified image of white boxed area (bottom right). Coronal section is taken at bregma + 3 mm (bottom left). Scale bars, 300 μm (top) and 50 μm (bottom). Throughout, error bars represent mean ± s.e.m. $^{*}P < 0.05$; $^{**}P < 0.01$; $^{***}P < 0.001$; $^{****}P < 0.0001$; n.s., not significant; by Student's t-test.

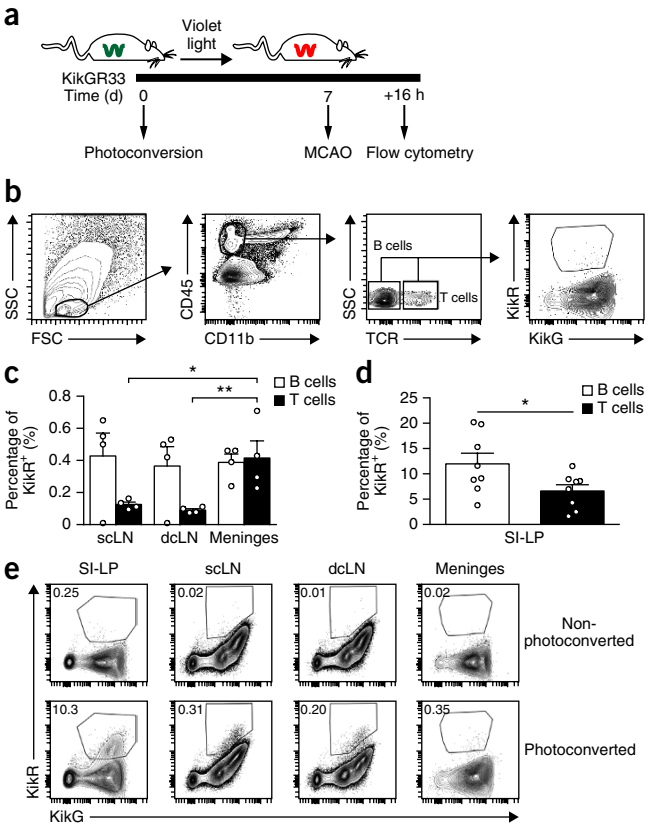

Figure 4 Migration of intestinal T cells to the meninges after ischemic brain injury. (**a**) Schematic for analysis of KikGR mice. Photoconversion of the distal part of the small intestine is induced using violet light 7 d before MCAO induction, and the photoconverted (KikR$^+$) cells are analyzed in different tissues by flow cytometry 16 h after MCAO induction. (**b**) Flow cytometric gating strategy in photoconverted KikGR mice. T cells (CD45$^+$CD11b$^-$TCR$^+$) and B cells (CD45$^+$CD11b$^-$TCR-β$^-$TCR-γδ$^-$) express the red variant of the protein (KikR$^+$) in the meninges 16 h after MCAO induction. (**c**) Frequency of photoconverted cells (KikR$^+$) relative to total numbers of B or T cells in superficial cervical lymph nodes (scLN; $n = 4$), deep cervical lymph nodes (dcLN; $n = 4$) and meninges ($n = 4$). One data point is derived from the analysis of cells pooled from three animals. Error bars represent mean ± s.e.m. $^*P < 0.05$ and $^{**}P < 0.01$; by one-way analysis of variance (ANOVA) and Tukey's test. (**d**) Proportion of KikR$^+$ B and T cells in the LP of the small intestine (SI-LP; $n = 8$). One data point is derived from one animal. Error bars represent mean ± s.e.m. $^*P < 0.05$; by Student's *t*-test. (**e**) Representative analysis of photoconverted CD45^{high}CD11b$^-$ cells in several organs, showing the different signals from a non-photoconverted (top; $n = 2$ per organ) and a photoconverted (bottom; $n = 4$ per organ) mouse 16 h after ischemia. The gates in the dot plots identify KikR$^+$ cells, and the numbers denote the percentage of KikR$^+$ cells relative to total CD45^{high}CD11b$^-$ lymphocytes.

protocol and performed sham surgery or MCAO. Sixteen hours later, before the ischemic infarct is fully established, we processed the brains and meninges for flow cytometric analysis. We detected only a few γδ T cells in the ischemic brain (data not shown) and found the bulk of γδ T cells in the meninges. The frequency of meningeal γδ T cells was increased after stroke, as compared to that in sham-operated mice (**Fig. 3d**), and IL-17 protein expression was higher in the γδ T cells of AC^{Res} mice after stroke as compared to that in the γδ T cells of AC^{Sens} mice, which were not different from sham-operated mice (**Fig. 3d**). We also observed T_{reg} cells in the meninges, but the cell numbers were not different between AC^{Res} and AC^{Sens} mice (**Supplementary Fig. 9**). To determine the precise location of the cells within the meningeal layers—including the dura mater, arachnoid and pia mater—we examined intact skull sections of mice expressing *GFP* under control of the endogenous T cell receptor delta chain (*Tcrd*) locus, using immunofluorescence. γδ T cells were localized to the leptomeninges 16 h after MCAO induction (**Fig. 3e**). Some GFP$^+$ γδ T cells were also observed in the choroid plexus, a point of central nervous system (CNS) entry for T cells[23], whereas the brain parenchyma was devoid of γδ T cells (data not shown).

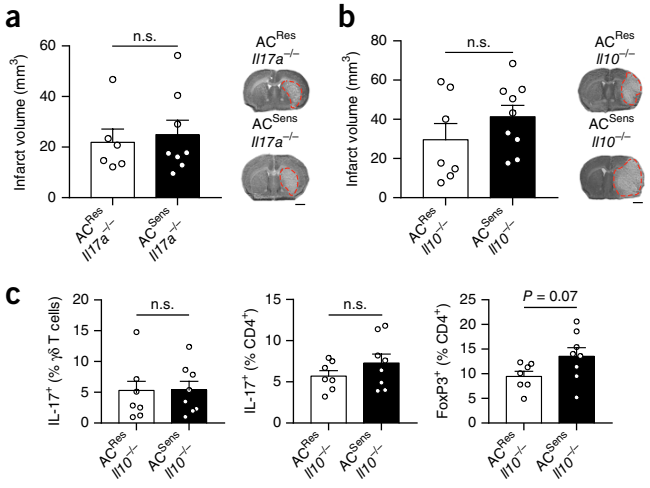

Figure 5 Neuroprotection conferred by intestinal dysbiosis requires a reduction in intestinal IL-17$^+$ γδ T cells. (**a**) Infarct volume in AC^{Res} ($n = 6$) and AC^{Sens} ($n = 8$) *Il17a*$^{-/-}$ mice (left), as measured by Nissl staining of coronal brain sections (representative images, right), 3 d after MCAO induction. Scale bar, 1 mm. (**b**) Left, infarct volume in AC^{Res} ($n = 7$) and AC^{Sens} ($n = 9$) *Il10*$^{-/-}$ mice on day 3 after MCAO induction. Right, representative coronal brain sections from *Il10*$^{-/-}$ AC^{Res} (top) and AC^{Sens} (bottom) mice with Nissl staining. Scale bar, 1 mm. (**c**) IL-17$^+$ γδ T cells (left), T_H17 cells (middle) and FoxP3$^+$ cells (right) in the LP of the small intestine of AC^{Res} ($n = 7$) and AC^{Sens} ($n = 8$) *Il10*$^{-/-}$ mice after 2 weeks of antibiotic treatment, as measured by flow cytometry. Throughout, error bars represent mean ± s.e.m. *P* values determined by Student's *t*-test; n.s., not significant.

Intestinal T cells traffic to the meninges after stroke

Recent studies have shown bidirectional trafficking of leukocytes between the intestine and secondary lymphoid organs[24]. Therefore we assessed whether T cells that have acquired a regulatory or effector phenotype in the gut could traffic to cervical lymph nodes (cLNs) and the meninges. We used KikGR33 mice, which ubiquitously express the Kikume Green-Red (KikGR) fluorescent protein that undergoes stable photoconversion from a green to a red form (which we refer to as KikG and KikR, respectively) after illumination with violet light[25]. We exposed the distal small intestine to violet light through a laparotomy, which resulted in efficient KikG to KikR conversion in gut-resident but not circulating immune cells (**Supplementary Fig. 10**). One week after photoconversion, we induced MCAO in these mice and analyzed the gut, superficial and deep cLNs, and meningeal immune cells by flow cytometry 16 h after stroke (**Fig. 4a,b**), a time point that precedes leukocyte infiltration into the brain (**Fig. 3a**). The frequency of KikR$^+$ T cells was higher in the meninges than in the superficial and deep cLNs, suggesting that gut-derived T cells preferentially home to the

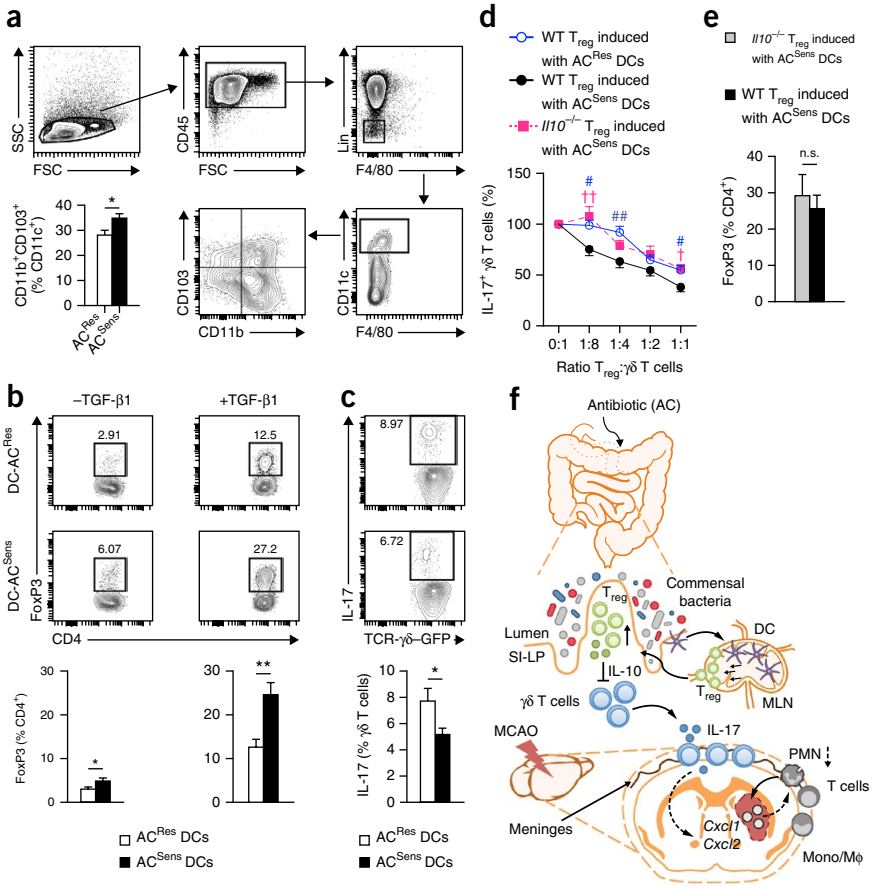

Figure 6 DCs from AC^{Sens} mice originate in the intestine, induce T_{reg} cells and downregulate IL-17$^+$ γδ T cells *in vitro*. (**a**) Flow cytometry analysis of DCs (CD45^{high}CD11c$^+$F4/80$^-$Lin$^-$; Lin, B220$^+$CD3-ε$^+$) isolated from mLNs of AC^{Sens} and AC^{Res} mice. Graph represents the percentages of CD11b$^+$CD103$^+$ subpopulations in CD11c$^+$ cells (n = 12 mice per group). (**b**) Top, representative flow cytometry analysis of T_{reg} cells (CD4$^+$FoxP3$^+$) cocultured with DCs from AC^{Res} or AC^{Sens} mice in the absence (AC^{Res}, n = 13 mice; AC^{Sens}, n = 16 mice) (left) or presence (AC^{Res}, n = 5 mice; AC^{Sens}, n = 6 mice) (right) of TGF-β1. Numbers in the dot plots are percentages of T_{reg} cells relative to total CD4$^+$ cells. Bottom, quantification of T_{reg} cells relative to total CD4$^+$ cells. (**c**) Top, representative flow cytometric analysis of IL-17 expression in γδ T cells cocultured with DCs from AC^{Res} (n = 10) or AC^{Sens} (n = 9) mice. Gates in the dot plots identify IL-17$^+$ γδ T cells, and the numbers are the percentage of IL-17$^+$ cells of total γδ T cells. Bottom, quantification of IL-17$^+$ γδ T cells, as analyzed by flow cytometry. (**d**) Suppression of IL-17$^+$ γδ T cells after coculture with T_{reg} cells generated *in vitro* by incubating CD4$^+$ cells from WT mice with DCs from AC^{Res} (n = 12–14 per data point) or AC^{Sens} mice (n = 11 per data point) and CD4$^+$ cells from *Il10*$^{-/-}$ mice with DCs from AC^{Sens} mice (n = 9 per data point). **Supplementary Table 4** shows the exact n values for each group and data point. (**e**) The percentage of T_{reg} cells induced by coculture of DCs from AC^{Sens} and CD4$^+$ cells from WT or *Il10*$^{-/-}$ mice (n = 6 independent experiments per group). (**f**) Proposed mechanism of protection from ischemic brain injury induced by intestinal microbial dysbiosis. Two weeks of AC treatment results in microbial dysbiosis. mLN DCs that originate in the small intestine induce T_{reg} cells. After homing to the gut, IL-10–secreting T_{reg} cells suppress IL-17$^+$ γδ T cell differentiation. Effector T cells traffic from the intestine to the meninges, where a reduction in IL-17$^+$ γδ T cells decreases post-ischemic chemokine (*Cxcl1* and *Cxcl2*) expression and leukocyte infiltration, improving outcome after brain ischemia. Throughout, error bars represent mean ± s.e.m. $^*P < 0.05$; $^{**}P < 0.01$; n.s., not significant; by Student's t-test. $^{\dagger}P < 0.05$; $^{\#}P < 0.05$; $^{\dagger\dagger}P < 0.05$; $^{\#\#}P < 0.01$; by one-way ANOVA.

meninges after stroke (**Fig. 4c**). The frequency of KikR$^+$ B cells did not differ among tissues. As expected, the frequency of KikR$^+$ T cells was highest in the intestine (**Fig. 4d**). The percentage of intestinal KikR$^+$ T cells was lower than that of KikR$^+$ B cells, suggesting that T cells may exit the small intestine LP at higher rates than B cells, as previously reported for the large intestine[24]. Almost no KikR$^+$ cell trafficking was observed in mice that underwent laparotomy but were not exposed to the light source (**Fig. 4e**).

Neuroprotection after dysbiosis depends on IL-17 and IL-10

Next we tested whether suppression of IL-17–producing immune cells in AC^{Sens} mice with the altered intestinal flora was sufficient to provide neuroprotection. *Il17a*$^{-/-}$ mice underwent either an AC^{Res} or an AC^{Sens} treatment protocol and were subjected to MCAO 2 weeks later. Infarct volumes were similar between AC^{Res} *Il17a*$^{-/-}$ and AC^{Sens} *Il17a*$^{-/-}$ mice, supporting an essential role for IL-17 in this model (**Fig. 5a**). Because our data indicates that the frequency of T_{reg} cells is increased in the small intestine of AC^{Sens} mice (**Fig. 2a**,**b**), we examined whether T_{reg} cells are involved in the suppression of IL-17$^+$ γδ T cells in our model. Because IL-10 is involved in T_{reg} cell–mediated inhibition of γδ T effector cells[14], we used IL-10–deficient (*Il10*$^{-/-}$) mice. Neuroprotection after stroke was not observed in AC-treated *Il10*$^{-/-}$ mice (**Fig. 5b**), and the frequency of IL-17$^+$ γδ T cells in the small intestine LP did not differ between groups (**Fig. 5c**). These findings reveal a link between intestinal T_{reg} cell expansion and IL-10–dependent reduction in IL-17$^+$ γδ T cells observed in AC^{Sens} mice.

Dendritic cell reprogramming affects T cell differentiation

To address whether local immune cell interactions are modified by intestinal dysbiosis, we examined the impact of the gut flora on the capacity of intestinal antigen-presenting cells to promote T_{reg} cell and IL-17$^+$ γδ T cell differentiation *in vitro*. Dendritic cells (DCs) sustain immune homeostasis in the intestine by inducing T_{reg} cells[26]. We investigated whether altering the intestinal microflora impacts T cell differentiation by modulating the activity of intestinal DCs. CD103$^+$ DCs originate in the intestinal LP and migrate to the mesenteric LN (mLN), where they drive the differentiation of gut-homing T_{reg} cells[26–28]. Consistent with a tolerogenic phenotype, we found that the percentage of CD11c$^+$CD11b$^+$CD103$^+$ DCs was higher in mLNs isolated from AC^{Sens} mice, as compared to those from AC^{Res} mice (**Fig. 6a**). We then isolated DCs from mLNs of both AC^{Res} and AC^{Sens} mice and tested their respective abilities to induce T_{reg} and IL-17$^+$ γδ T cell differentiation. In cocultures with CD4$^+$ T cells, DCs from AC^{Sens} mice were more efficient than DCs from AC^{Res} mice in inducing T_{reg} cell differentiation (**Fig. 6b**). After coculture with γδ T cells, DCs from AC^{Res} mice were more effective at inducing IL-17$^+$ γδ T cells than DCs from AC^{Sens} mice (**Fig. 6c**), suggesting that the commensal bacteria alter DC function.

IL-10 is required for T_{reg} cell–mediated IL-17$^+$ γδ T cell suppression

Next we tested whether T_{reg} cells can suppress IL-17$^+$ γδ T cell differentiation *in vitro*. Increasing numbers of T_{reg} cells, generated by coculturing CD4$^+$ T cells with DCs isolated from mLNs of AC^{Sens} or AC^{Res} mice, were cocultured with naive γδ T cells. T_{reg} cells suppressed IL-17$^+$ γδ T differentiation in a dose-dependent manner, and T_{reg} cells from cocultures with DCs from AC^{Sens} mice were more efficient than T_{reg} cells obtained from cocultures with DCs from AC^{Res} mice (**Fig. 6d**). To test whether the suppression was mediated by IL-10, we compared T_{reg} cells generated by coculturing DCs from AC^{Sens} mice with CD4$^+$ T cells isolated from wild-type (WT) or *Il10*$^{-/-}$ mice. IL-10 deficiency reduced the capacity of T_{reg} cells to suppress IL-17$^+$ γδ T differentiation (**Fig. 6d**), even though the numbers of *Il10*$^{-/-}$ T_{reg} cells were comparable to the number of WT T_{reg} cells (**Fig. 6e**).

DISCUSSION

Our study describes a novel microbiota-gut-brain axis that is based on the observation that bacterial priming of intestinal DCs leads to expansion of local T_{reg} cells in the small intestine and suppression of effector IL-17$^+$ γδ T cell function. The data suggest that effector T cells traffic from the gut to the brain, where they localize in the leptomeninges and enhance ischemic neuroinflammation by secreting IL-17; this results in increased chemokine production in the brain parenchyma and subsequent infiltration of cytotoxic immune cells, including neutrophils (**Fig. 6f**).

We found that DCs isolated from the mLNs of AC^{Sens} mice were more efficient in inducing T_{reg} cells than DCs isolated from the mLNs of AC^{Res} mice, suggesting antigen-dependent imprinting. DCs can directly sample intestinal content[29,30] and migrate to the mLN, where they present antigens to induce T_{reg} polarization[26]. Consistent with the importance of this mechanism, we found that DCs in the mLNs of AC^{Sens} mice expressed higher levels of CD103, a marker of tolerogenic intestinal DCs[26–28]. As compared to T_{reg} cell induction, the ability of DCs from AC^{Sens} mice to suppress IL-17$^+$ γδ T cell generation was less striking, suggesting that T_{reg} cell induction could be the main mechanism by which DCs suppress IL-17$^+$ γδ T cells. Accordingly, we found that T_{reg} cells generated in cocultures with DCs from AC^{Sens} mice inhibited IL-17$^+$ γδ T differentiation more efficiently than T_{reg} cells generated by DCs from AC^{Res} mice. In line with previous findings that identified IL-10 as a critical factor for T_{reg} cell–mediated γδ T cell suppression[14], we found that *Il10*$^{-/-}$ T_{reg} cells generated by coculture with DCs from AC^{Sens} mice were less efficient in suppressing IL-17$^+$ γδ T differentiation than WT T_{reg} cells. The suppressive activity of T_{reg} cells was not completely abolished, indicating that other mechanisms not affected by intestinal dysbiosis also have a role. This is to be expected because the involvement of IL-10 is only one of the possible mechanisms by which T_{reg} cells suppress T cell proliferation[31]. Notably, the decrease of suppressive activity in *Il10*$^{-/-}$ T_{reg} cells was similar to that in WT T_{reg} cells derived from cocultures with DCs from AC^{Res} mice, indicating that most of the dysbiosis-induced effects on IL-17$^+$ γδ T are IL-10 dependent. Accordingly, dysbiosis was unable to confer neuroprotection in *Il10*$^{-/-}$ mice.

A new and unexpected finding of our study is the trafficking of intestinal T cells to the meninges. T cells are known to patrol the body, including the brain, where they enter through the choroid plexus into the cerebrospinal fluid[23] and probably drain through a recently described meningeal lymphatic system to the deep cervical lymph nodes[32]. Intestinal T cells have been found to traffic to extra-intestinal LNs and the spleen[24]. However, our data show that intestinal T cells preferentially accumulate in the meninges as opposed to the cervical LNs after stroke, suggesting directed gut-brain trafficking. Whereas the frequency of T_{reg} cells was increased in the small intestine of mice with dysbiosis, T_{reg} cell numbers in the meninges were not increased. Although the evidence for a direct protective effect of brain-associated T_{reg} cells remains controversial[8,18,33,34], our data indicate that T_{reg} cells might affect stroke outcome—independently of their presence in the brain and meninges—through an intestinal mechanism involving IL-17$^+$ γδ T cell suppression. We also show that the meninges function as a gatekeeper in post-ischemic inflammation. This is evidenced by the observation that γδ T cells did not enter the brain after stroke but remained restricted to the leptomeninges, where their numbers increased after stroke. Because inflammatory cells might enter the injured brain through extravasation from compromised meningeal vessels[35,36], meningeal IL-17$^+$ γδ T cells would be at a strategic location to control the trafficking of monocytes and neutrophils—the main leukocyte populations found in the ischemic brain—to the brain parenchyma. In support of this interpretation, we found fewer IL-17$^+$ γδ T cells in the meninges after stroke in mice with intestinal dysbiosis, and this was associated with reduced IL-17–responsive chemokine expression in the brain parenchyma. Although the role of γδ T cells as contributing factor to ischemic brain injury is not supported in all models[37], here we identify IL-17$^+$ γδ T cells as the probable effector T cell that is regulated by intestinal dysbiosis. Because we found changes in T_{reg} and IL-17$^+$ γδ T cell frequencies in the small intestine but not in the colon, peripheral blood, spleen and LNs of AC-treated mice, alteration of the bacterial composition in the small intestine could account for this effect. The bacterial species responsible for the immune changes in the gut that underlie the protective effect of dysbiosis remain to be identified. AC treatment resulted in a profound alteration of intestinal microbiota—which was characterized by a retraction of Clostridiaceae and S24-7 spp., a major family of Bacteroidetes, and a concomitant expansion of Proteobacteria. Clostridiaceae and S24-7 Bacteroidetes were also reduced in mice receiving fecal transplants from AC^{Sens} donors, raising the possibility that a reduction in members of these bacterial families could be involved in neuroprotection. Studies to identify the relevant bacterial species are ongoing.

IL-17 and γδ T cells have also been implicated in human stroke. Infiltration of γδ T cells and secretion of IL-17 have been documented in ischemic human brain tissue[7,38]. Circulating IL-17 is increased in stroke patients[39], and IL-17 expression in atherosclerotic lesions is associated with increased plaque vulnerability, a known risk factor for embolic stroke[40]. Given that several anti–IL-17 drugs are in clinical trials for a variety of inflammatory disorders (https://clinicaltrials.gov/), the use of such drugs in clinical stroke seams feasible, after pharmacokinetic and safety data become available. Although no epidemiological data linking intestinal microbiota with the risk or outcome of stroke are available as yet, inflammatory bowel disease and Crohn's disease—both of which have been linked to altered gut flora and increased intestinal IL-17 production[19,41]—have been identified as risk factors for stroke[42,43], suggesting that the microbiota–IL-17$^+$ γδ T cell–brain axis identified in our mouse studies might also exist in humans.

In conclusion, our findings shed new light on poorly understood immune mechanisms that have an impact on brain injury and have far-reaching and translationally relevant implications for assessing cerebrovascular risk and predicting stroke severity.

METHODS

Methods and any associated references are available in the online version of the paper.

Note: Any Supplementary Information and Source Data files are available in the online version of the paper.

ACKNOWLEDGMENTS

J.A. is the recipient of the Finbar and Marianne Kenny Research Scholarship. Parts of the study were supported by the US National Institutes of Health (NIH) grants NS081179 (J.A.) and NS34179 (C.I. and J.A.), the Feil Family Foundation (C.I.) and the Swiss National Science Foundation for Grants in Biology and Medicine (P3SMP3 148367; C.B.). We thank A.-K. Hadjantonakis (Memorial Sloan Kettering Cancer Center) for helpful discussions on the use of the KikGR33 mice.

AUTHOR CONTRIBUTIONS

C.B. and D.B. contributed to study design, performed and/or contributed critically to all experiments and analyzed data. In some experiments, C.B. and D.B. were assisted by J.M., M.M., G.S. and G.R. G.F. performed EB extravasation experiments. E.G.P. and S.C. developed and provided the AC^{Res} mouse model. L.L. performed r16S sequencing, and together with E.G.P., analyzed taxonomic data. C.I. contributed to study design. J.A. formulated the original hypothesis, designed the study, analyzed data and wrote the manuscript together with C.B., D.B. and C.I. All authors read and approved the manuscript.

COMPETING FINANCIAL INTERESTS

The authors declare no competing financial interests.

1. Henninger, N., Kumar, R. & Fisher, M. Acute ischemic stroke therapy. *Expert Rev. Cardiovasc. Ther.* **8**, 1389–1398 (2010).
2. Iadecola, C. & Anrather, J. The immunology of stroke: from mechanisms to translation. *Nat. Med.* **17**, 796–808 (2011).
3. Macrez, R. *et al.* Stroke and the immune system: from pathophysiology to new therapeutic strategies. *Lancet Neurol.* **10**, 471–480 (2011).
4. Mazmanian, S.K., Liu, C.H., Tzianabos, A.O. & Kasper, D.L. An immunomodulatory molecule of symbiotic bacteria directs maturation of the host immune system. *Cell* **122**, 107–118 (2005).
5. Prinz, I., Silva-Santos, B. & Pennington, D.J. Functional development of γδ T cells. *Eur. J. Immunol.* **43**, 1988–1994 (2013).
6. Shichita, T. *et al.* Pivotal role of cerebral interleukin-17–producing γδ T cells in the delayed phase of ischemic brain injury. *Nat. Med.* **15**, 946–950 (2009).
7. Gelderblom, M. *et al.* Neutralization of the IL-17 axis diminishes neutrophil invasion and protects from ischemic stroke. *Blood* **120**, 3793–3802 (2012).
8. Liesz, A., Hu, X., Kleinschnitz, C. & Offner, H. Functional role of regulatory lymphocytes in stroke: facts and controversies. *Stroke* **46**, 1422–1430 (2015).
9. Liesz, A. *et al.* Regulatory T cells are key cerebroprotective immunomodulators in acute experimental stroke. *Nat. Med.* **15**, 192–199 (2009).
10. Stubbe, T. *et al.* Regulatory T cells accumulate and proliferate in the ischemic hemisphere for up to 30 days after MCAO. *J. Cereb. Blood Flow Metab.* **33**, 37–47 (2013).
11. Li, P. *et al.* Adoptive regulatory T cell therapy protects against cerebral ischemia. *Ann. Neurol.* **74**, 458–471 (2013).
12. Chaudhry, A. *et al.* $CD4^+$ regulatory T cells control T_H17 responses in a Stat3-dependent manner. *Science* **326**, 986–991 (2009).
13. Huber, S. *et al.* T_H17 cells express interleukin-10 receptor and are controlled by $Foxp3^-$ and $Foxp3^+$ regulatory $CD4^+$ T cells in an interleukin-10–dependent manner. *Immunity* **34**, 554–565 (2011).
14. Park, S.-G. *et al.* T regulatory cells maintain intestinal homeostasis by suppressing γδ T cells. *Immunity* **33**, 791–803 (2010).
15. Cho, S. *et al.* The class B scavenger receptor CD36 mediates free radical production and tissue injury in cerebral ischemia. *J. Neurosci.* **25**, 2504–2512 (2005).
16. Kunz, A. *et al.* Neurovascular protection by ischemic tolerance: role of nitric oxide and reactive oxygen species. *J. Neurosci.* **27**, 7083–7093 (2007).
17. Braniste, V. *et al.* The gut microbiota influences blood-brain barrier permeability in mice. *Sci. Transl. Med.* **6**, 263ra158 (2014).
18. Hu, X., Li, P. & Chen, J. Pro: regulatory T cells are protective in ischemic stroke. *Stroke* **44**, e85–e86 (2013).
19. Round, J.L. & Mazmanian, S.K. The gut microbiota shapes intestinal immune responses during health and disease. *Nat. Rev. Immunol.* **9**, 313–323 (2009).
20. Nishio, J. & Honda, K. Immunoregulation by the gut microbiota. *Cell. Mol. Life Sci.* **69**, 3635–3650 (2012).
21. Justicia, C. *et al.* Neutrophil infiltration increases matrix metalloproteinase–9 in the ischemic brain after occlusion-reperfusion of the middle cerebral artery in rats. *J. Cereb. Blood Flow Metab.* **23**, 1430–1440 (2003).
22. Stowe, A.M. *et al.* Neutrophil elastase and neurovascular injury following focal stroke and reperfusion. *Neurobiol. Dis.* **35**, 82–90 (2009).
23. Engelhardt, B. & Ransohoff, R.M. The ins and outs of T lymphocyte trafficking to the CNS: anatomical sites and molecular mechanisms. *Trends Immunol.* **26**, 485–495 (2005).
24. Morton, A.M. *et al.* Endoscopic photoconversion reveals unexpectedly broad leukocyte trafficking to and from the gut. *Proc. Natl. Acad. Sci. USA* **111**, 6696–6701 (2014).
25. Nowotschin, S. & Hadjantonakis, A.-K. Use of KikGR, a photoconvertible green-to-red fluorescent protein, for cell labeling and lineage analysis in ES cells and mouse embryos. *BMC Dev. Biol.* **9**, 49 (2009).
26. Coombes, J.L. *et al.* A functionally specialized population of mucosal $CD103^+$ DCs induces $Foxp3^+$ regulatory T cells via a TGF-β– and retinoic acid–dependent mechanism. *J. Exp. Med.* **204**, 1757–1764 (2007).
27. Scott, C.L., Aumeunier, A.M. & Mowat, A.M. Intestinal $CD103^+$ dendritic cells: master regulators of tolerance? *Trends Immunol.* **32**, 412–419 (2011).
28. Ochoa-Repáraz, J. *et al.* A polysaccharide from the human commensal *Bacteroides fragilis* protects against CNS demyelinating disease. *Mucosal Immunol.* **3**, 487–495 (2010).
29. Rescigno, M. *et al.* Dendritic cells express tight-junction proteins and penetrate gut epithelial monolayers to sample bacteria. *Nat. Immunol.* **2**, 361–367 (2001).
30. Niess, J.H. *et al.* CX3CR1-mediated dendritic cell access to the intestinal lumen and bacterial clearance. *Science* **307**, 254–258 (2005).
31. Josefowicz, S.Z., Lu, L.-F. & Rudensky, A.Y. Regulatory T cells: mechanisms of differentiation and function. *Annu. Rev. Immunol.* **30**, 531–564 (2012).
32. Louveau, A. *et al.* Structural and functional features of central nervous system lymphatic vessels. *Nature* **523**, 337–341 (2015).
33. Kleinschnitz, C. & Wiendl, H. Con: regulatory T cells are protective in ischemic stroke. *Stroke* **44**, e87–e88 (2013).
34. Kleinschnitz, C. *et al.* Regulatory T cells are strong promoters of acute ischemic stroke in mice by inducing dysfunction of the cerebral microvasculature. *Blood* **121**, 679–691 (2013).
35. Roth, T.L. *et al.* Transcranial amelioration of inflammation and cell death after brain injury. *Nature* **505**, 223–228 (2014).
36. Pérez-de-Puig, I. *et al.* Neutrophil recruitment to the brain in mouse and human ischemic stroke. *Acta Neuropathol.* **129**, 239–257 (2015).
37. Kleinschnitz, C. *et al.* Early detrimental T cell effects in experimental cerebral ischemia are neither related to adaptive immunity nor to thrombus formation. *Blood* **115**, 3835–3842 (2010).
38. Li, G.-Z. *et al.* Expression of interleukin-17 in ischemic brain tissue. *Scand. J. Immunol.* **62**, 481–486 (2005).
39. Kostulas, N., Pelidou, S.H., Kivisäkk, P., Kostulas, V. & Link, H. Increased IL-1β, IL-8 and IL-17 mRNA expression in blood mononuclear cells observed in a prospective ischemic stroke study. *Stroke* **30**, 2174–2179 (1999).
40. Erbel, C. *et al.* Expression of IL-17A in human atherosclerotic lesions is associated with increased inflammation and plaque vulnerability. *Basic Res. Cardiol.* **106**, 125–134 (2011).
41. Abraham, C. & Cho, J. Interleukin-23–T_H17 pathways and inflammatory bowel disease. *Inflamm. Bowel Dis.* **15**, 1090–1100 (2009).
42. Keller, J.J. *et al.* Increased risk of stroke among patients with Crohn's disease: a population-based matched cohort study. *Int. J. Colorectal Dis.* **30**, 645–653 (2015).
43. Singh, S., Kullo, I.J., Pardi, D.S. & Loftus, E.V. Jr. Epidemiology, risk factors and management of cardiovascular diseases in IBD. *Nat. Rev. Gastroenterol. Hepatol.* **12**, 26–35 (2015).

ONLINE METHODS

Mice. All procedures were approved by the institutional animal care and use committee of Weill Cornell Medical College (Animal protocol number: 2012-0051). Wild-type C57BL/6, *Il10*$^{-/-}$ (B6.129P2-Il10tm1Cgn/J), *Il17a*$^{-/-}$ (Il17atm1.1(icre)Stck/J), *Il17a-eGFP* (C57BL/6-Il17atm1Bcgen/J), *Trdc-eGFP* (C57BL/6-Trdctm1Mal/J) and KikGR33 (Tg(CAG-KikGR)33Hadj/J) mice were purchased from Jackson Laboratories (JAX; Bar Harbor, Maine, USA). Genetically modified lines were bred in our facility. All mice were males on a C57BL/6 background except for KikGR33 mice, which were on a mixed C57BL/6–ICR background and for which male and female mice were used. All animal experiments were performed in accordance with the 'animal research: reporting of *in vivo* experiments' (ARRIVE) guidelines[44].

Mouse husbandry. Specific-pathogen-free (SPF) C57BL/6 mice (males; age = 6 weeks) were purchased from Jackson Laboratories and allowed to acclimatize in the animal facility for 1 week before being randomly assigned to experimental groups. The SPF status of the facility is continuously monitored with sentinel animals by the veterinary service of Weill Cornell Medical College. JAX C57BL/6 mice do not harbor segmented filamentous bacteria (SFB), a known inducer of T_H17 cells in mice[45]. JAX mice and mice derived from our housing facility and used for this study were negative for SFB by r16S sequencing of fecal pellets and by qPCR using SFB-specific primers[46,47]. All mice were housed under a 12-h light cycle in autoclaved microisolator cages, with individual sterile air supply, on autoclaved bedding and drinking water, and with sterilized standard chow *ad libitum*. To minimize maternal effects on microbiota composition[48,49], mice from different litters were pooled before randomly assigning them to experimental groups.

Antibiotic treatment. C57BL/6 mice (males, 7 weeks old) and *Il10*$^{-/-}$, *Il17a*$^{-/-}$, *Il17a-eGFP* and *Trdc-eGFP* mice (males, 7–8 weeks old) received 1 g/liter of amoxicillin (a β-lactam antibiotic)–clavulanic acid (a β-lactamase inhibitor) (AC; West-Ward Pharmaceutical Corp., Eatontown, NJ) in autoclaved tap water for 1 or 2 weeks. Mice weighing less than 20 g at the beginning of the treatment were excluded from the study. All mice were housed in the same room and randomly allocated into two groups: AC-resistant (AC^{Res}) mice co-housed for 2 weeks with an AC^{Res} seeder mouse or AC-sensitive (AC^{Sens}) mice. Additional mice were treated with water alone (H_2O) or with vancomycin (0.5 g/liter; Gold Biotechnology, St. Louis, MO) for 2 weeks. Administration of vancomycin was discontinued 3 d before inducing middle cerebral artery occlusion (MCAO) to avoid off-target effects of antibiotics. Bottles with antibiotic-containing water were inverted every day, and the antibiotic solution was changed every 3–4 d, together with the cage bedding. To prevent bacterial cross-contamination, mouse handling and biweekly cage changes were performed by technicians wearing a clean gown and gloves in a ventilated hood.

Fecal microbial transplantation. Cecal contents were pooled from two donor mice. According to Caricilli *et al.*[50] with slight modifications, cecal content was resuspended in PBS prepared in autoclaved tap water (2.5 ml/cecum), filtered using a strainer and stored at −80 °C until use. To facilitate colonization of the transplanted flora, recipient mice were pulse-treated for 3 d with AC before administration of 200 µl of cecal extract by oral gavage. Transplanted mice were kept on nonmedicated water for 2 weeks after fecal transplantation until MCAO induction.

Middle cerebral artery occlusion. Transient focal cerebral ischemia was induced using the intraluminal filament model of MCAO, as described elsewhere[51]. Briefly, mice were anesthetized with 1.5–2% isoflurane, and rectal temperature was maintained at 37 ± 0.5 °C throughout surgery. A heat-blunted nylon suture (6/0) was inserted into the right external carotid artery and advanced until it obstructed the MCA together with the ligation of the common carotid artery for 35 min. Regional cerebral blood flow (CBF, bregma coordinates: 2-mm posterior, 5-mm lateral) was continuously recorded by transcranial laser Doppler flowmetry (Periflux System 5010; Perimed, King Park, NY) from the induction of ischemia until 30 min after reperfusion. We only included mice that had a residual CBF <15% throughout the ischemic period and CBF recovery >80% within 10 min of reperfusion. Following MCAO, mice were placed in temperature-controlled recovery cages for 2 h to prevent post-surgery hypothermia. The order in which mice from different groups were subjected to MCAO was randomized. AC^{Sens} mice cannot be blinded to the investigator because they have an enlarged abdomen and their stool pellets appear distinguishable from those of AC^{Res} mice. **Supplementary Table 2** indicates the number of mice excluded and the percentage of survival after MCAO.

Measurement of infarct volume. Mice were euthanized 3 d after ischemia. Brains were frozen on dry ice and serially sectioned (600-µm intervals, 30-µm thick) for cresyl violet staining. Infarct volume, corrected for swelling[52], was quantified using an image analysis software (MCID; Imaging Research) by an investigator blinded to the treatment.

Behavioral testing. Sensorimotor deficits were assessed 3 and 7 d after MCAO by the contact and removal adhesive tape test[53]. Mice were tested at the start of the dark phase of the circadian day-night cycle. Briefly, an adhesive tape 0.3 × 0.4 cm (Band-Aid, flexible fabric, Johnson and Johnson) was placed on the dorsal aspect of both forepaws. Time duration of tape contact with the mouth and tape removal was scored on videos recorded over 180 s. At the beginning of each testing session, mice were allowed to acclimate for 1 min in a glass cylinder covered by white paper. For training purposes, 2 d before MCAO induction, mice performed the test four times with 5- to 10-min rest cycles in the home cage between individual trials. Mice that were not able to remove the tape after training were excluded from the study (AC^{Res}, $n = 2$; AC^{Sens}, $n = 0$). Post-MCAO trials were conducted two times for 180 s each time to diminish stress effects related to handling. Results were expressed as mean of the two trials of either the contralateral contact or removal time. The sequence in which mice from different treatment groups were assessed was randomly assigned. AC^{Sens} mice cannot be blinded to the investigator because they show an enlarged abdomen and their stool pellets appear distinguishable from those of AC^{Res} mice.

Intact skull immunohistochemistry. Mice were anesthetized with isoflurane and perfused transcardially with ice-cold PBS followed by 4% paraformaldehyde (PFA). After removing the mandibles, the skin and muscles were carefully detached from the skull (http://www.nature.com/protocolexchange/protocols/3389). The skull decalcification was performed as previously described[54]. Coronal consecutive sections (10-µm thick) were cut using a cryostat set at a temperature of −23 °C. Skull sections were permeabilized with PBS and 0.5% Triton X-100, blocked with normal goat serum and incubated overnight at 4 °C with rabbit polyclonal anti–mouse pan-laminin antibody (1:200; Z0097, DAKO) followed by Alexa Fluor 546–conjugated goat anti–rabbit secondary antibody (1:200; Molecular Probes, Invitrogen Corporation, Carlsbad, CA, USA). Sections were counterstained with TO-PRO-3 (Invitrogen) to visualize cell nuclei and observed by confocal laser microscopy (Leica SP5).

Blood-brain barrier permeability by Evans Blue dye extravasation. Evans Blue (EB) dye (2%; 100 µl) was injected intravenously into the jugular vein of naive AC^{Res} and AC^{Sens} mice or 5 h after reperfusion in mice undergoing middle cerebral artery occlusion[55]. After 1 h of circulation, mice were perfused transcardially with ice-cold PBS. The brain stem and cerebellum were discarded and the forebrains were separated into ipsilateral and contralateral hemispheres. Samples were weighed, frozen on dry ice and stored at −80 °C. Forebrains were homogenized in 500 µl of PBS, mixed with 500 µl of trichloroacetic acid and centrifuged. Supernatants were diluted four times with ethanol, and samples were read in triplicate on a fluorescence plate reader (620-nm excitation, 680-nm emission). A standard curve was obtained using 0–500 ng/ml EB. Values were normalized for the weight difference by dividing each sample value (ng/ml) by the respective weight. Data are expressed as a ratio of EB dye in ipsilateral hemisphere/ EB dye in contralateral hemisphere (IH/CH).

Stool sample collection and DNA extraction. To avoid the confounding effects of co-housing on the diversity of the intestinal microbiota for each treatment group, we collected samples from mice housed in different cages. Fresh stool pellets were collected and stored at −80 °C. Frozen stool samples (~100 mg) were placed in sterile polypropylene microvials (BioSpec Products) containing 1 ml InhibitEX Buffer (QIAGEN), 1 ml of 0.1-mm diameter

doi:10.1038/nm.4068

zirconia-silica beads (BioSpec Products) and one 3.5-mm diameter glass bead (Biospec Products). Samples were homogenized for 2 min using a Mini-BeadBeater 16 (BioSpec Products). DNA was purified with the QIAamp Fast DNA Stool Mini Kit (QIAGEN) according to the manufacturer's instructions.

Quantification of 16S ribosomal (r16S) DNA copy numbers. r16S DNA sequences were amplified from stool DNA using 0.2 µM of the universal bacterial r16S gene primers 16S-V2-101F (5′-AGYGGCGIACGGGTGAGTAA-3′) and 16S-V2-361R (5′-CYIACTGCTGCCTCCCGTAG-3′) in conjunction with Maxima SYBR Green/ROX qPCR Master mix 2× (Thermo Scientific). Amplifications were performed on a Chromo 4 Detector (Bio-Rad, Hercules, CA) using a two-step cycling protocol consisting of: 50 °C for 2 min, 95 °C for 10 min, followed by 45 cycles of 95 °C for 15 s, 60 °C for 1 min. The standard curve was prepared using a plasmid containing an *Escherichia coli* r16S V2 DNA fragment.

16S rRNA gene amplification and multiparallel sequencing. Amplicons of the V4-V5 16S rRNA region were amplified and sequenced using an Illumina MiSeq platform. For each sample, duplicate 50-µl PCR reactions were performed, each containing 50 ng of purified DNA, 0.2 mM dNTPs, 1.5 mM $MgCl_2$, 2.5 U Platinum Taq DNA polymerase, 2.5 µl of 10× PCR buffer, and 0.5 µM of each primer designed to amplify the V4-V5: 563F (5′-nnnnnnnn-NNNNNNNNNNN-AYTGGGYDTAAAGNG-3′) and 926R (5′-nnnnnnnn-NNNNNNNNNNN-CCGTCAATTYHTTTRAGT-3′). A unique 12-base Golay barcode (Ns) preceded the primers to allow sample identification, and 1–8 additional nucleotides were placed in front of the barcode to offset the sequencing of the primers. Cycling conditions were 94 °C for 3 min, followed by 27 cycles of 94 °C for 50 s, 51 °C for 30 s, and 72 °C for 1 min. A condition of 72 °C for 5 min was used for the final elongation step. Replicate PCRs were pooled, and amplicons were purified using the QIAquick PCR Purification Kit (QIAGEN). PCR products were quantified and pooled at equimolar amounts before ligation of Illumina barcodes and adaptors according to Illumina TruSeq Sample Preparation protocol. The completed library was sequenced on an Illumina MiSeq platform following the Illumina-recommended procedures.

Sequence analysis. Sequences were analyzed using the mothur pipeline, version 1.33.3 (ref. 56) as described previously[57]. Sequences with a distance-based similarity of 97% or greater were grouped into operational taxonomic units (OTUs) using the furthest-neighbor algorithm and classified using a modified in-house database containing sequences from GreenGenes 99 and retrieved 16S sequences from Genbank; OTU-based microbial diversity was estimated by calculating the nonparametric Shannon diversity index (α-diversity). Sequence-abundance profiles in each sample were used for downstream statistical and modeling analysis. A phylogenetic tree was inferred using Clearcut[58] on the 16S rRNA sequence alignment generated by mothur.

Quantitative determination of mRNA in brain tissue. A 4-mm slice of the ipsilateral forebrain was collected 24 h after middle cerebral artery occlusion and snap-frozen in liquid nitrogen. The mRNA for chemokine (C-X-C motif) ligand genes *Cxcl1* and *Cxcl2* were examined by qRT-PCR as previously described[59]. Hypoxanthine guanine phosphoribosyl transferase (*Hprt*) was used to normalize gene expression. Tissue was homogenized using a bead homogenizer (BioSpec Bartlesville, OK) with stainless steel beads in TRIzol Reagent (Invitrogen Life Technologies, Grand Island, NY) and RNA was extracted according to the manufacturer's instructions. RNA samples were treated with RNase-free DNaseI (Roche, Indianapolis, IN) to remove DNA contamination. cDNA was produced from mRNA samples by using the RevertAid First Strand cDNA Synthesis Kit (Thermo Fisher Scientific, Waltham, MA). All primers were purchased from Invitrogen Life Technologies (Grand Island, NY). Primer sequences were as follows (Invitrogen): *Cxcl1*, 5′-GCGAAAAGAAGTGCAGAGAGA-3′ and 5′-AAACACAGCCTCCCACACAT-3′; *Cxcl2*, 5′-TGAACAAAGGCAAGGCTAACTG-3′ and 5′-GAGGCAC ATCAGGTACGATCC-3′ and *Hprt*, 5′-AGTGTTGGATACAGGCCAGAC-3′ and 5′-CGTGATTCAAATCCCTGAAGT-3′. qRT-PCR was conducted with 3 µl of cDNA (1:10 dilution), in duplicate 15-µl reactions using the Maxima SYBR Green/ROX qPCR Master Mix (2×) (Thermo Fisher Scientific, Waltham, MA). The reactions were incubated at 50 °C for 2 min and then at 95 °C for 10 min. A PCR cycling protocol consisting of 15 s at 95 °C and 1 min at 60 °C for 45 cycles was used for quantification. *Cxcl1* and *Cxcl2* relative expression levels were calculated by $2^{(-\Delta\Delta C_T)}$ method. Data were expressed as mean fold change in the ischemic hemisphere relative to that in the naive brain.

Cell isolation from lymphoid organs and blood. The spleen, mesenteric, axillary, inguinal deep and superficial cervical lymph nodes (LNs) were isolated and placed on a premoistened 70-µm cell strainer. All lymphoid organs were then gently homogenized with the end of a 1-ml syringe plunger. LN cells were eluted from the strainer with 10 ml PBS. For spleens, the strainer was washed with 10 ml erythrocyte lysis buffer (150 mM NH_4Cl, 1 mM $KHCO_3$, 0.1 mM EDTA; pH 7.2), and the eluted cells were incubated for 5 min at room temperature and washed with 40 ml PBS. Blood was drained from the submandibular vein into tubes containing sodium heparin, incubated for 5 min at room temperature with erythrocyte lysis buffer, followed by addition of 10 ml of Hank's balanced salt solution (HBSS) with 10 mM HEPES. Cell suspensions were centrifuged at 500*g* for 7 min and subsequently stained for flow cytometric analysis, or stimulated *in vitro* for analysis of intracellular cytokines.

Cell isolation from mesenteric lymph nodes for dendritic cell analysis. For dendritic cell analysis, mesenteric lymph nodes were isolated and digested with 5 ml HBSS with 10 mM HEPES, containing 5% FBS and 0.2 mg/ml collagenase D (Sigma). Tissue was digested at 37 °C for 20 min with constant agitation (250 r.p.m.), then vigorously vortexed for 20 s. The resulting cell suspension was filtered through a 40-µm nylon cell strainer and washed with 10 ml PBS. Cell suspensions were centrifuged at 500*g* for 7 min and subsequently stained for flow cytometric analysis.

Isolation of intestinal intraepithelial lymphocytes (IELs) and lamina propria mononuclear cells (LPMCs). Mice were sacrificed by pentobarbital overdose (Sigma; 200 mg per kg body weight (mg/kg); i.p.). Small and large intestines were removed and separated. Peyer's patches were excised, and intestines were cleaned of mesenteric fat and intestinal contents. Then intestines were opened longitudinally, washed with PBS, cut into ~1-cm pieces and placed into 20 ml of HBSS with 10 mM HEPES, 8% FBS, 4 mM EDTA, 0.5 mM dithiothreitol. Tissue pieces were washed three times in a shaking incubator set at 250 r.p.m. and 37 °C for 20 min. After each round, tissue suspension was vortexed for 20 s, and the supernatant containing the IELs was collected. Supernatants were combined and filtered first over 0.3 g of premoistened nylon wool placed in a 10-ml syringe and then over a 70-µm strainer. Remaining tissue pieces were washed with Ca^{2+}-Mg^{2+}-PBS to remove EDTA, minced thoroughly, and placed into 5 ml HBSS with 10 mM HEPES containing 5% FBS and 0.2 mg/ml collagenase D (Sigma). Tissue was digested at 37 °C for 20 min with constant agitation (250 r.p.m.), then vigorously vortexed for 20 s. The resulting cell suspension containing LPMCs was filtered through a 40-µm nylon cell strainer and washed with 10 ml PBS. IEL and LPMC cell suspensions were collected at 500*g* for 10 min at 4 °C. Cell pellets were resuspended in 8 ml 44% Percoll (GE healthcare, #57-0891-01) and overlaid over 5 ml of 67% Percoll. Gradients were centrifuged at 500*g* for 20 min at 4 °C and cells at the interface were collected and washed with 10 ml PBS. Cells were stained for flow cytometric analysis or used for *in vitro* stimulation.

Isolation of brain leukocytes. Isolation of brain leukocytes was performed according to Pino *et al.*[60]. Briefly, mice were anesthetized with pentobarbital and transcardially perfused with 20 ml cold PBS. Brains were removed, olfactory bulbs and cerebellum excised, and hemispheres separated. One hemisphere was placed in a douncer containing 3 ml RPMI-1640 medium (Sigma) with phenol red and gently homogenized. Then 4 ml of RPMI-1640 and 3 ml of 100% Percoll (final concentration 30% Percoll) were added and overlaid over 2 ml of 70% Percoll. Gradients were centrifuged at 500*g*, for 30 min at 18 °C. Cells were recovered from the interface, washed twice with PBS and either stained for flow cytometric analysis or used for *in vitro* stimulation.

Meningeal cell isolation. Mice were anesthetized with pentobarbital and transcardially perfused with 20 ml cold PBS. The upper portion of the skull was separated from the brain and the meninges were recovered from the interior of the

skull bones, using a dissection microscope. Meninges were placed on the surface of a premoistened 70-µm cell strainer. Tissue was gently homogenized with the end of a 1-ml syringe plunger, washed with 10 ml PBS and centrifuged at 500*g* for 7 min. Cells were either stained for flow cytometric analysis or stimulated *in vitro* for analysis of intracellular cytokines.

Flow cytometry analysis. For surface marker analysis, cell suspensions were adjusted to a density of 1×10^6 cells in 50 µl FACS buffer (2% FBS, 0.05% NaN_3 in PBS). Nonspecific binding was blocked by incubation for 10 min at 4 °C with anti–CD16-CD32 antibody (BioLegend, clone 93, 5 ng/µl) and stained with the appropriate antibodies for 15 min at 4 °C. The following antibodies were used for extracellular staining: CD45 (clone 30F-11, 0.5 ng/µl), CD4 (clone RM4-5, 0.5 ng/µl), TCR-β (clone H57-597, 4 ng/µl), TCR-γδ (clone GL3, 4 ng/µl), CD11b (clone M1/70, 0.6 ng/µl), Ly6G (clone 1A8, 2 ng/µl), CD11c (clone N418, 2 ng/µl), NK1.1 (clone PK136, 0.32 ng/µl), CD19 (clone 6D5, 0.6 ng/µl), CD103 (clone 2E7, 1.5 ng/µl), F4/80 (clone BM8, 0.5 ng/µl), B220 (clone RA3-6B2, 0.32 ng/µl) and CD3-ε (clone 145-2C11, 2 ng/µl) from BioLegend. For intracellular staining, cells were first stained for surface markers as detailed above, fixed and permeabilized using Fixation and Permeabilization buffers from eBiosciences following the manufacturer's instructions. Briefly, cells were fixed for 30 min at 4 °C, washed with Permeabilization Buffer and incubated for 30 min with the appropriate antibodies in Permeabilization Buffer at 4 °C. The following antibodies were used: FoxP3 (clone FJK-16s, 0.5 ng/µl) and IL-17A (clone eBio17B7, 1 ng/µl) from eBiosciences. Cells were washed with FACS buffer, resuspended in 200 µl of FACS buffer and analyzed with a MACSQuant10 cytometer (Myltenyi Biotec). Analysis was performed with FlowJo software (version 10, Tree Star). Gates were validated by TO-PRO-3 and fluorescein-diacetate labeling to identify dead and live cells, respectively. Isotype controls, single antibody–stained samples and 'fluorescence – 1' controls were used to establish compensation and gating parameters[61]. Samples were acquired and analyzed by an investigator blinded to the treatment groups.

***In vitro* stimulation for intracellular IL-17 expression analysis.** For IL-17 analysis, we used either *Il17a-GFP* reporter mice or anti–IL-17 antibodies in wild-type mice. Cells pooled from two animals were resuspended in RPMI-1640 medium containing 10% FBS, 100 ng/ml phorbol 12-myristate 13-acetate (PMA) and 1 µg/ml ionomycin. Brefeldin (3 µg/ml, Sigma) was added for intracellular IL-17 staining. Cells were incubated for 4 h at 37 °C, and then washed and stained as indicated above for flow cytometric analysis.

Photoconversion of KikGR mice. Mice were anesthetized with 2.5% isoflurane (vol/vol), delivered in 2 liter/min of 30% O_2 and 70% N_2O, and maintained at 37 °C throughout the procedure. Photoconversion was performed with a defocused (1.5-cm beam diameter) violet laser source (405 nm, peak power 4.5 mW, ThorLabs) essentially as described[24]. Briefly, mice were placed in a supine position and covered with an aluminum foil blanket. A 3-cm incision was made into the abdominal wall, exposing the distal part of the small intestine. The exposed gut segment (~6 cm) was illuminated for 20 min through an opening in the aluminum foil covering the animal. Intestinal tissue was kept hydrated by applying saline throughout the procedure. The intestine was returned to the abdominal cavity, and the peritoneum and skin were sutured closed. 7 d after photoconversion, mice were subjected to MCAO, and 16 h later mice were anesthetized with pentobarbital intraperitoneally and transcardially perfused with 20 ml cold PBS. The deep and superficial LNs, meninges and LPMC from small intestine were extracted and prepared as previously indicated for flow cytometric analysis (three animals were pooled), and the percentage of photoconverted red cells ($KikR^+$) was analyzed in B and T cell populations.

Isolation of dendritic cells, $CD4^+$ cells and γδ T cells. Mice were sacrificed by pentobarbital overdose. Mesenteric lymph nodes (LNs) were extracted and digested for 20 min at 37 °C with collagenase type IV (0.2 mg/ml; Sigma) in HBSS with 10 mM HEPES and 5% of FBS. Cell suspension was enriched for $CD11c^+$ cells by positive selection on MS-MACS columns (Miltenyi Biotec) using an anti-CD11c–PE antibody (clone N418) and anti-PE microbeads (purity >75%). CD4 T cells were isolated by incubating splenocytes with the following biotinylated antibodies: CD8a (clone 53-6.7, 187 ng/µl), B220 (clone RA3-6B2, 47 ng/µl), CD49b (clone Hma2, 94 ng/µl), CD11b (clone M1/70, 94 ng/µl) and TER119 (clone TER119, 38 ng/µl) (BioLegend; except for anti-CD49b (eBiosciences)). This was followed by anti-biotin microbeads and negative enrichment with LS-MACS columns according to the manufacturer's instructions (Miltenyi Biotec). Purity was consistently >95%. γδ T cells were isolated from the spleen and LNs of *Trdc-eGFP* mice. Three or four mice were pooled for each γδ T isolation. Splenocytes and LN cells were prepared as described above and incubated with the following biotinylated antibodies: TCR-β (clone H57-597, 187 ng/µl), B220 (clone RA3-6B2, 47 ng/µl), CD49b (clone Hma2, 94 ng/µl), CD11b (clone M1/70, 94 ng/µl) and TER119 (clone TER119, 38 ng/µl) (BioLegend, except for anti-CD49b (eBiosciences)). This was followed by anti-biotin microbeads and negative selection with LS-MACS columns according to the manufacturer's specifications (Miltenyi Biotec) (purity >65%).

***In vitro* induction of regulatory T cells.** Mesenteric lymph node dendritic cells (DCs) isolated from AC^{Res} and AC^{Sens} mice were cultured with $CD4^+$ cells from naive mice (2.5×10^4 DCs and 2.5×10^4 $CD4^+$ cells per well in 96-well plates), in RPMI 1640 medium with 10% FBS, 2 mM L-glutamine, 30 µM β-mercaptoethanol, non-essential amino acids (NEAAs), 1 mM sodium pyruvate, penicillin-streptomycin together with 1 µg/ml anti-CD3 (clone 17A2) and 100 U/ml of IL-2 (BioLegend) for 3 d, either with or without TGF-β1 (1 ng/ml, PreproTech). Cells were washed with FACS buffer, blocked with CD16- and CD32-specific antibodies for 10 min at 4 °C and stained with CD45-specific and TCR-β–specific antibodies for 15 min at 4 °C. Cells were fixed and permeabilized for 30 min at 4 °C and then intracellularly stained with FoxP3-specific antibody for 30 min at 4 °C for flow cytometric analysis. The percentage of $FoxP3^+$ cells in the $CD4^+$ cell population ($CD45^+TCR\text{-}\beta^+CD4^+$) was calculated.

***In vitro* induction of IL-17–producing γδ T cells.** Mesenteric lymph node dendritic cells (DCs) isolated from AC^{Res} and AC^{Sens} mice were cultured with γδ T cells from naive *Trdc-eGFP* mice for 3 d (2.5×10^4 DCs and 2.5×10^4 γδ T cells per well in 96-well plates precoated with 10 µg/ml of TCR-γδ antibody (clone GL4)) in RPMI-1640 medium with 10% FBS, 2 mM L-glutamine, 30 µM β-mercaptoethanol, NEAAs, 1 mM sodium pyruvate and penicillin-streptomycin. Then cells were washed with fresh medium and resuspended in RPMI-1640 medium containing 10% FBS, 100 ng/ml PMA, 1 µg/ml ionomycin and brefeldin (3 µg/ml, Sigma), incubated for 4 h at 37 °C, and then washed and stained as previously indicated for flow cytometric analysis; the percentage of $IL\text{-}17^+$ cells in the γδ T cell population was calculated.

***In vitro* suppression of IL-17–producing γδ T cells.** T_{reg} cells were induced as described above by coculturing $CD4^+$ cells from naive wild-type or $Il10^{-/-}$ mice with AC^{Res} or AC^{Sens} DCs. At day 3 of culture, cells were collected and $CD4^+$ cells were isolated by negative selection. Cells were cocultured at different ratios (0:1, 1:8, 1:4, 1:2 and 1:1) with γδ T cells (2.5×10^4 cells), which were freshly isolated from naive *Trdc-eGFP* mice, in 96-well plates precoated with 10 µg/ml of TCR-γδ antibody (clone GL4) in RPMI-1640 medium with 10% FBS, 2 mM L-glutamine, 30 µM β-mercaptoethanol, NEAAs, 1 mM sodium pyruvate and penicillin-streptomycin for 4 d. Then cells were washed and restimulated as described above. Cells were washed with FACS buffer, blocked with an antibody to CD16 and CD32 and stained with antibodies to CD45 and TCR-β. Cells were fixed and permeabilized for 30 min and intracellularly stained with anti–IL-17 antibody for 30 min at 4 °C for flow cytometric analysis. The number of $IL\text{-}17^+$ cells in the γδ T cell population ($CD45^+TCR\text{-}\beta^-TCR\text{-}\delta\text{–}GFP^+$) was calculated and normalized to $IL\text{-}17^+$ γδ T cell numbers in the control group (ratio T_{reg} cells:γδ T cells of 0:1).

Statistical analysis. Mouse randomization was based on the random number generator function (RANDBETWEEN) in Microsoft Excel software. GraphPad Prism (v. 6.0) software was used for statistical analysis. Data are expressed as mean ± s.e.m. and were analyzed by unpaired Student's *t*-test (two-tailed) or one-way ANOVA and Tukey's test, as appropriate. When variances were different, the Welch's correction for unequal variances was applied to the Student's *t*-tests. Comparison of survival percentages between groups was analyzed by the Fisher's exact test. Exclusion criteria are described in the individual method sections. Predictor OTUs were identified by 'random forest' classification using the OTU frequency matrix

doi:10.1038/nm.4068

at the family level as predictors and infarct volume as the response vector. Analysis was run in R (v. 3.2.3) with the library randomForest[62] (v. 4.6-10) in unsupervised mode with 500 trees and importance as the output.

44. Kilkenny, C., Browne, W., Cuthill, I.C., Emerson, M. & Altman, D.G. Animal research: reporting *in vivo* experiments—the ARRIVE guidelines. *J. Cereb. Blood Flow Metab.* **31**, 991–993 (2011).
45. Ivanov, I.I. *et al.* Induction of intestinal T_H17 cells by segmented filamentous bacteria. *Cell* **139**, 485–498 (2009).
46. Snel, J. *et al.* Comparison of 16S rRNA sequences of segmented filamentous bacteria isolated from mice, rats and chickens, and proposal of '*Candidatus arthromitus*'. *Int. J. Syst. Bacteriol.* **45**, 780–782 (1995).
47. Barman, M. *et al.* Enteric salmonellosis disrupts the microbial ecology of the murine gastrointestinal tract. *Infect. Immun.* **76**, 907–915 (2008).
48. Benson, A.K. *et al.* Individuality in gut microbiota composition is a complex polygenic trait shaped by multiple environmental and host genetic factors. *Proc. Natl. Acad. Sci. USA* **107**, 18933–18938 (2010).
49. Ubeda, C. *et al.* Familial transmission rather than defective innate immunity shapes the distinct intestinal microbiota of TLR-deficient mice. *J. Exp. Med.* **209**, 1445–1456 (2012).
50. Caricilli, A.M. *et al.* Gut microbiota is a key modulator of insulin resistance in *Tlr2*-knockout mice. *PLoS Biol.* **9**, e1001212 (2011).
51. Jackman, K., Kunz, A. & Iadecola, C. Modeling focal cerebral ischemia *in vivo*. *Methods Mol. Biol.* **793**, 195–209 (2011).
52. Lin, T.N., He, Y.Y., Wu, G., Khan, M. & Hsu, C.Y. Effect of brain edema on infarct volume in a focal cerebral ischemia model in rats. *Stroke* **24**, 117–121 (1993).
53. Bouët, V. *et al.* Sensorimotor and cognitive deficits after transient middle cerebral artery occlusion in the mouse. *Exp. Neurol.* **203**, 555–567 (2007).
54. Yagi, S. & Costanzo, R.M. Grafting the olfactory epithelium to the olfactory bulb. *Am. J. Rhinol. Allergy* **23**, 239–243 (2009).
55. Jackman, K. *et al.* Progranulin deficiency promotes post-ischemic blood-brain barrier disruption. *J. Neurosci.* **33**, 19579–19589 (2013).
56. Schloss, P.D. *et al.* Introducing mothur: open-source, platform-independent, community-supported software for describing and comparing microbial communities. *Appl. Environ. Microbiol.* **75**, 7537–7541 (2009).
57. Buffie, C.G. *et al.* Precision microbiome reconstitution restores bile acid–mediated resistance to *Clostridium difficile*. *Nature* **517**, 205–208 (2015).
58. Sheneman, L., Evans, J. & Foster, J.A. Clearcut: a fast implementation of relaxed neighbor joining. *Bioinformatics* **22**, 2823–2824 (2006).
59. Garcia-Bonilla, L., Racchumi, G., Murphy, M., Anrather, J. & Iadecola, C. Endothelial CD36 contributes to postischemic brain injury by promoting neutrophil activation via CSF3. *J. Neurosci.* **35**, 14783–14793 (2015).
60. Pino, P.A. & Cardona, A.E. Isolation of brain and spinal cord mononuclear cells using Percoll gradients. *J. Vis. Exp.* **48**, 2348 (2011).
61. Roederer, M. Spectral compensation for flow cytometry: visualization artifacts, limitations and caveats. *Cytometry* **45**, 194–205 (2001).
62. Liaw, A. & Wiener, M. Classification and regression by randomForest. *R News* **2**, 18–22 (2002).